Molecular Simulation
Vol. 35, No. 6, May 2009, 466–472

Taylor & Francis
Taylor & Francis Group

Molecular simulation of the nanoscale water confined between an atomic force microscope tip and a surface

H.J. Choi[a], J.Y. Kim[a], S.D. Hong[a], M.Y. Ha[a] and J. Jang[b]*

[a]*School of Mechanical Engineering, Pusan National University, Busan, South Korea;* [b]*Department of Nanomaterials Engineering, Pusan National University, Miryang, South Korea*

(*Received 19 October 2008; final version received 19 November 2008*)

Under ambient humidity, water condenses as a nanometre meniscus between an atomic force microscope (AFM) tip and a surface, giving rise to a strong capillary force on the tip. To examine the molecular features of the meniscus, we performed an all-atom molecular dynamics simulation. By varying the tip–surface distance, we have simulated the formation, thinning and snap-off of the water meniscus. The meniscus is several nanometres wide and substantially fluctuates in its periphery when its neck is narrow. The density profile of the meniscus shows that its periphery is not sharp but has a fuzzy boundary whose thickness ranges from 0.4 to 0.9 nm. We obtained the neck radius of the meniscus and the radius of curvature of its periphery. Due to the sharp asperity of the AFM tip, these two structural parameters are comparable in size, in contrast to the case of a macroscopic tip, where the neck radius is much greater. We found that the meniscus periphery is often far from a circle in shape. With the structural parameters of the meniscus, we calculated the capillary force by using the Laplace–Kelvin equation. Our calculation reproduces the typical behaviour of the force–distance curve in the AFM experiment.

Keywords: water meniscus; capillary force; AFM; molecular dynamics simulation

1. Introduction

It is well known that water naturally condenses between an atomic force microscope (AFM) tip and a surface under ambient conditions [1–3]. This is a manifestation of the capillary condensation of water vapour under spatial confinement between solids (i.e., the tip and the surface) [4,5]. This nanoscale water meniscus gives rise to a significant adhesion force on the order of nN which must be supplied to retract the tip from the surface [6–9]. This pull-off force is frequently measured as a function of humidity [7–9]. The water meniscus also serves as a channel for molecules to flow from an AFM tip to a surface in dip-pen nanolithography [10]. Considering the widespread applications of the AFM tip in surface science and nanotechnology, it is important to understand the meniscus and the resulting capillary force at the molecular level.

A theoretical study, obviating experimental uncertainty and complication, is expected to provide clear insights into the meniscus and the capillary force. In predicting the shape of the meniscus, the most widely used is the Laplace–Kelvin equation [4,11],

$$RT \ln (p/p_0) = \gamma V \left(\frac{1}{r_1} + \frac{1}{r_2} \right), \qquad (1)$$

where p is the pressure, p_0 the saturation pressure of water vapour, T the temperature, γ the surface tension ($=0.0726\,\mathrm{N/m}$), and $V(=1.8 \times 10^{-5}\,\mathrm{m^3/mol})$ the molar volume of liquid water. As sketched in Figure 1, r_2 in Equation (1) is the neck radius of the meniscus (a cylindrical symmetry of meniscus assumed) and r_1 is the radius of curvature of the meniscus periphery. r_1 is negative for a concave meniscus but positive for a convex one. Equation (1) is frequently used to predict the meniscus shape for a given relative humidity p/p_0. However, it should be pointed out that the Laplace–Kelvin Equation (1) alone cannot determine two unknown structural parameters r_1 and r_2 simultaneously. It is then generally assumed that r_2 is much greater than r_1, and only r_1 is determined. In the case of a macroscopic tip, the tip can be approximated as a plane due to its large radius. Then the resulting meniscus is wide so that the above assumption is valid. In the case of nanoscale menisci, however, there is no guarantee that the assumption $r_2 \gg |r_1|$ holds. Instead, r_2 and r_1 can be comparable in magnitude. Furthermore, the Laplace–Kelvin equation usually predicts little humidity dependence of the capillary force, in contradiction to many measurements. Therefore, Xiao and Qian [9] conclude that the Laplace–Kelvin theory is not able to reproduce the experimental behaviour of the pull-off force with respect to humidity.

In our viewpoint, the most severe shortcoming of continuum theory like Equation (1) is its inability to deliver molecular insights of the problem. For example, a water meniscus becomes often unstable when the tip diameter is small (such as for a carbon nanotube tip) and

*Corresponding author. Email: jkjang@pusan.ac.kr

ISSN 0892-7022 print/ISSN 1029-0435 online

DOI: 10.1080/08927020802635129
http://www.informaworld.com

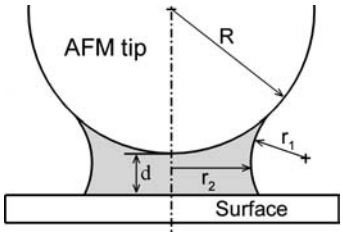

Figure 1. A schematic sketch of the water meniscus condensed between an AFM tip and a surface. The hemispherical tip has a radius R, and its end is separated from the surface by a distance d. The meniscus has a cylindrical symmetry around the tip axis. The meniscus has a radius of r_2 at neck and its periphery has a concave shape with a radius of curvature r_1 (<0).

the meniscus is only a few molecules wide [12]. Previously, we have performed grand canonical Monte Carlo simulations based on a lattice gas model [12–14]. This lattice model was able to capture the essential features of nanoscale confined water [15]. Our simulations reproduce the typical magnitude of the experimental capillary force and its humidity dependence. We have explored the roles of surface roughness and hydrophilicity on the capillary force. Our lattice model, however, misses some of the interesting molecular features of water such as its V-shaped geometry, dipole moment and long-ranged electrostatic interaction. Herein, we perform an all-atom molecular dynamics (MD) simulation to grasp a fully molecular picture of the meniscus. By obtaining the density profile of the water meniscus, we investigate the meniscus structure and its stability. We study how the meniscus varies as the tip retracts from a surface. We also obtain the structural parameters r_2 and r_1 from the density profile. Using these parameters, we further calculate the capillary force as a function of the tip–surface distance. We finally study how the hydrophilicity of surface affects the capillary force. We note in the passing that Cramer et al. [16] recently reported an MD simulation of a nanometre water meniscus at the molecular level. They studied the formation of a water pillar on a surface induced by an applied electric field. By contrast, the water bridge studied here is induced by the spatial confinement between the tip and the surface.

2. Simulation details

The AFM tip and surface consist of atoms which interact through Lennard-Jones (LJ) potential [17],

$$U(r) = 4\varepsilon[(\sigma/r)^{12} - (\sigma/r)^{6}]. \quad (2)$$

σ s for the tip and surface atoms are both identical to that of carbon. But we systematically vary the energetic parameter ε for the tip and surface atoms (see below). The tip geometry is taken to be a hemispherical shell of atoms. We initially set up a face-centred cubic (FCC) crystal with a lattice spacing equal to 0.321 nm (similar to the σ parameter of carbon). Then we choose the lattice points close to the smooth hemispherical surface with a radius of 13 nm. The resulting AFM tip is made up of 8282 atoms. Similarly, we generate the surface by picking up the top two layers of (111) surface of the same FCC used in the tip generation. Our surface consists of 4976 LJ atoms. Initially, a total of 1906 water molecules are placed on a finite cubic grid placed between the AFM tip and surface. The tip and surface atoms are fixed during simulation, so that we do not calculate the interaction between the tip and the surface. They, however, interact with water molecules confined between them.

For the water–water intermolecular interaction, we use TIP3P model [18]. Briefly, three atom-centred point charges (-0.834 on O and $+0.417$ on H) interact with each other through the Coulomb potential. The oxygen–oxygen interaction has an additional LJ potential, epsilon and sigma of which are 0.1521 kcal/mol and 0.35365 nm, respectively. We use the particle mesh Ewald method with a grid spacing of 0.1 nm [19] to calculate the long-ranged electrostatic interactions between partial charges. The molecular geometry of water is rigid: the oxygen–hydrogen bond length is 0.09572 nm and the angle between two O—H bonds is 104.52°. We use the SHAKE [17] algorithm to keep the water molecules rigid. The LJ interactions between different atomic species i and j (e.g. between a tip atom and water oxygen) are calculated by using Lorentz–Berthelot mixing rule [17]

$$\varepsilon_{ij} = \sqrt{\varepsilon_i \varepsilon_j}, \quad \sigma_{ij} = (\sigma_i + \sigma_j)/2. \quad (3)$$

We use the velocity Verlet algorithm for the propagation of MD trajectories [17]. Temperature was held constant at room temperature (300 K) by applying Langevin dynamics [20] method with a damping coefficient of 5 ps^{-1}. The MD time step is taken to be 1 fs and the typical length of the MD trajectory is 1 ns. We apply the periodic boundary conditions by using a simulation box with a volume of 15 nm × 15 nm × 15 nm. This box has a size big enough to remove any artefacts due to the interaction with self-images. This is confirmed by the additional simulation without the periodic boundary conditions, which shows the same structure in the meniscus as in the present work. We use the NAMD simulation package for conducting our MD simulation [21].

We have studied the formation, thinning and snap-off of the water meniscus by varying the distance between the AFM tip and the surface, d (Figure 1), from 1.4 to 3.7 nm. In addition, we have systematically varied the water–tip and water–surface interaction energies. That is, we have considered three LJ epsilon values for the tip atom, $\varepsilon_T = 0.1$, 2.0 and 2.5 kcal/mol. According to Equation (3), the corresponding LJ epsilon values for the tip–oxygen interaction ε_{TO} s are 0.123, 0.551 and 0.617 kcal/mol,

respectively. In the lattice gas model [12–14,22], the ratio of fluid–wall versus fluid–fluid interaction determines the wettability of the fluid on the wall. If the ratio is greater than 1, the wall is completely wet by the fluid, but if it is less than 1, the wall is either partially wet or completely dry. Similarly, we call the case of $\varepsilon_{TO} = 0.123$ kcal/mol a hydrophobic tip because ε_{TO} here is smaller than the LJ epsilon parameter of the water–water interaction, $\varepsilon_{OO}(= 0.1521$ kcal/mol). The tips with $\varepsilon_T = 2.0$ and 2.5 kcal/mol have $\varepsilon_{TO}/\varepsilon_{OO} = 3.6$ and 4.1, respectively, and can be called hydrophilic. The LJ epsilon parameter of the surface atom, ε_S, is varied as 0.1, 0.5, 1.0, 2.0 and 2.5 kcal/mol. Then the ratio of LJ epsilon parameter for the surface–oxygen interaction ε_{SO} relative to ε_{OO}, $\varepsilon_{SO}/\varepsilon_{OO}$, varies as 0.8, 1.8, 2.6, 3.6 and 4.1. As in the tip case, a hydrophobic (hydrophilic) surface has $\varepsilon_{SO}/\varepsilon_{OO}$ less (greater) than 1.

By collecting MD snapshots, we calculate the density profile ρ defined as the average number of water molecules at a given position. The density profile ρ is assumed cylindrically symmetric so that ρ is a function of the horizontal distance from the tip axis r and the vertical height from the surface h. In calculation of ρ, we use the MD trajectory after the initial 0.4 ns part. We normalise the density profile so that its highest value is scaled to be one. The bin sizes of the density profile in the horizontal and vertical directions, dr and dh, are 0.25 and 0.15 nm, respectively. We define the meniscus periphery as the contour line with 0.5 in the density profile. Then, assuming the meniscus periphery to be a circle, we determined the radius of curvature r_1 by using a nonlinear fitting of the half-density contour line.

3. Results and discussions

Figure 2 illustrates how the simulated water meniscus responds to the change in the tip–surface distance. Representative MD snapshots are drawn for the tip–surface distances of 1.4 nm (Figure 2(a)) and 3.7 nm (Figure 2(b)). Both the tip and the surface are hydrophilic ($\varepsilon_{TO}/\varepsilon_{OO} = \varepsilon_{SO}/\varepsilon_{OO} = 3.6$). The meniscus shrinks in width (almost nine times smaller) as the tip retracts from the surface. Regardless of the tip–surface distance, the meniscus retains its concave shape although its curvature changes little bit. In the case of $d = 3.7$ nm, the meniscus periphery does not look like a circle but rather a parabola. One can also see some holes in the meniscus. The meniscus is not as condensed as in $d = 1.4$, probably due to the thermal instability of the meniscus with a narrow width. Note also that, for both the tip–surface distances, the meniscus neck radius is comparable in size with the radius of curvature of the meniscus periphery. In the case of $d = 3.7$ nm, the neck radius is actually smaller than the radius of curvature.

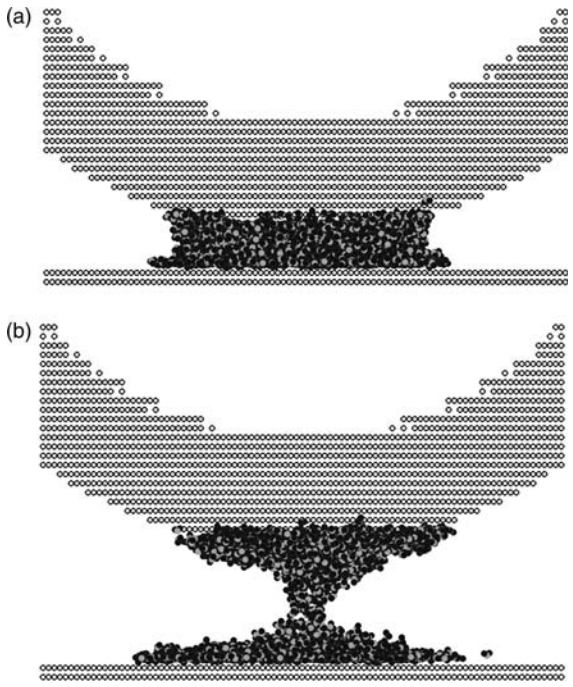

Figure 2. Molecular dynamics simulation snapshots of water menisci for two different tip–surface distances, 1.4 nm (a) and 3.7 nm (b). The tip and surface are both hydrophilic ($\varepsilon_{TO}/\varepsilon_{OO} = \varepsilon_{SO}/\varepsilon_{OO} = 3.6$). Tip and surface atoms are drawn as open circles. The hydrogen and oxygen atoms are drawn as black and grey spheres, respectively.

To quantitatively analyse the meniscus structure, we have calculated the density profile ρ as described in the Section 2. In Figure 3, we draw ρ as a contour plot for the tip–surface distances of 1.6 nm (Figure 3(a)) and 3.7 nm (Figure 3(b)). The meniscus periphery is defined as the half-density contour line drawn as a broken line. From this periphery, we calculated the radius at the neck, r_2. The neck radius reduces from 3.25 nm (Figure 3(a)) to 0.4 nm (Figure 3(b)) as the tip (the solid line) retracts from the surface. The meniscus is concave ($r_1 < 0$) regardless of d because both the tip and the surface are hydrophilic ($\varepsilon_{TO}/\varepsilon_{OO} = \varepsilon_{SO}/\varepsilon_{OO} = 3.6$). We found r_1 is -0.7 nm for $d = 1.6$ nm [Figure 3(a)] and -0.8 nm for $d = 3.7$ nm [Figure 3(b)]. Therefore, r_2 is comparable to r_1 for these nanomenisci, and the assumption $r_2 \gg \|r_1\|$ is not valid. Note that the density profile changes rather smoothly from liquid ($\rho = 1$) to vapour ($\rho = 0$). Therefore, the meniscus periphery is not infinitely sharp as is often assumed in thermodynamic theories. This fuzziness of the periphery can be related to the thermal instability (fluctuation) of the meniscus at the molecular level. To quantify the fuzziness, we have defined the thickness of periphery as the distance between $\rho = 0.75$ and $\rho = 0.25$ contour lines. The periphery thicknesses calculated this way are 0.44 nm and 0.9 nm for $d = 1.6$ and 3.7 nm, respectively. If we describe the meniscus width at neck as a statistical

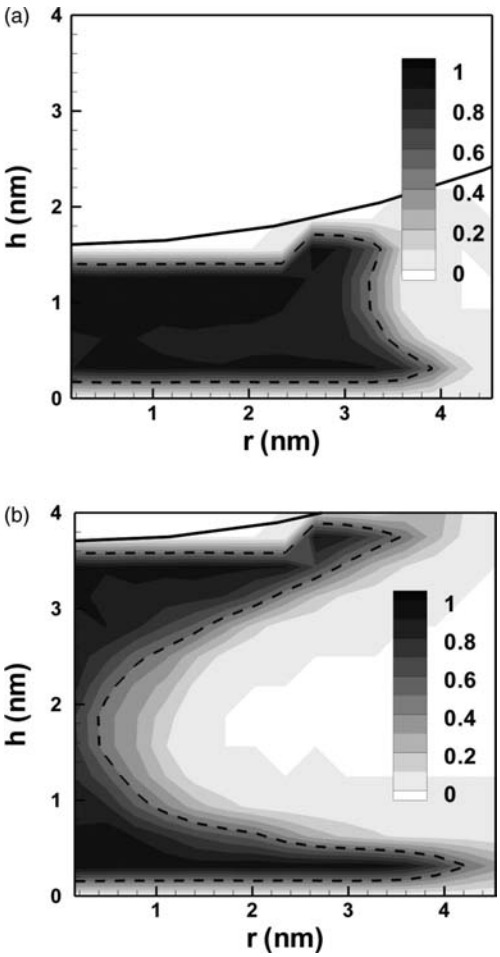

Figure 3. Change in the density profile of the water meniscus as the tip retracts from the surface. For two different tip–surface distances of 1.6 nm (a) and 3.7 nm (b), the density $\rho(r,h)$ is contour plotted as a function of the horizontal distance from the tip axis r and the vertical distance from the surface h. The tip boundary is drawn as a solid line. The dashed line represents the contour line of 0.5, which is taken to be the periphery of the meniscus. Both the tip and surface are hydrophilic ($\varepsilon_{TO}/\varepsilon_{OO} = \varepsilon_{SO}/\varepsilon_{OO} = 3.6$).

variable, we can interpret the above thickness as the fluctuation in the width and $2r_2$ as the average of the width. According to this notion, the fluctuation (0.9 nm) in the meniscus width becomes greater than its average (0.8 nm) in the case of $d = 3.7$ nm.

We determined the structural parameters of the meniscus for various tip–surface distances. Figure 4 shows how r_2 changes with an increase in the tip–surface distance d. As discussed above, we define the distance between 0.25 and 0.75 contour lines of the density profile as the fluctuation in r_2. In Figure 4, this fluctuation is drawn as error bars. Overall, the neck radius decreases as the tip–surface distance increases. At some short distances ($d = 2.9$, 3.1, 3.4 and 3.7 nm), r_2 shows a large error bar due to thermal instability of a narrow meniscus. In these

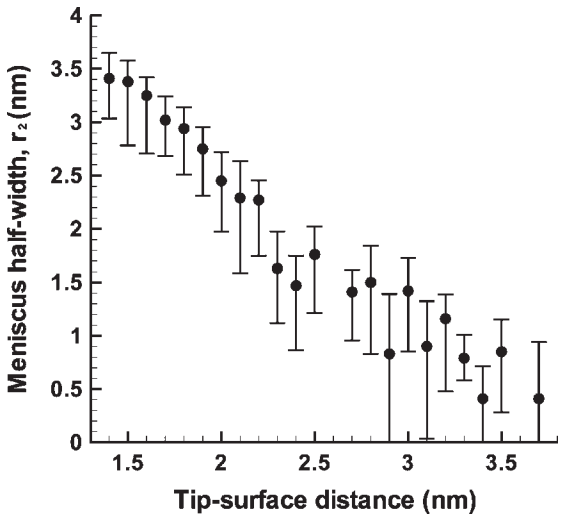

Figure 4. The neck radius of the water meniscus r_2 versus the tip–surface distance d. For each tip–surface distance, r_2 (drawn as circles) is estimated from the density profile as in Figure 3. Error bars represent the fluctuation in r_2 defined as the distance between the contour lines of 0.25 and 0.75 in the density. Both the tip and the surface are hydrophilic ($\varepsilon_{TO}/\varepsilon_{OO} = \varepsilon_{SO}/\varepsilon_{OO} = 3.6$).

cases, the system is largely fluctuating and perhaps its thermodynamics state is near a liquid–vapour phase transition. To get a more statistically accurate result for r_2 then, we might need to run a significantly longer simulation than the present work. Here, we content ourselves with the fact that, within the statistical accuracy represented as error bars, our simulation gives a decreasing r_2 with respect to the increase in d.

Once we obtain r_1 and r_2 from the density profile, we can calculate the capillary force $F(d)$ for a given tip–surface distance d by using [23]

$$F(d) = \gamma\left(\frac{1}{r_1} + \frac{1}{r_2}\right) \times \pi r_2^2. \tag{4}$$

As we pointed out already, the two radii in Equation (4) are comparable in size for nanoscale menisci simulated in the work. A convex (positive r_1) meniscus will always result in a repulsive (positive in sign) force. A concave (negative r_1) meniscus is likely to result in an attractive (negative in sign) force. However, Equation (4) tells us that, if r_2 is smaller than r_1 in magnitude, even a concave meniscus can yield a repulsive fore. Since the capillary force in Equation (4) is a function of r_2, it is subject to fluctuation, if there is a fluctuation in r_2. Using the fluctuation in r_2 drawn in Figure 3, we calculated the resulting fluctuation in capillary force. Only the fluctuation in r_2 (but not in r_1) is included in obtaining the force fluctuation. Figure 5 shows the capillary force versus the tip–surface distance. The fluctuation in force is drawn as error bars. The figure captures the essential features of the force–distance curve obtained in a typical AFM

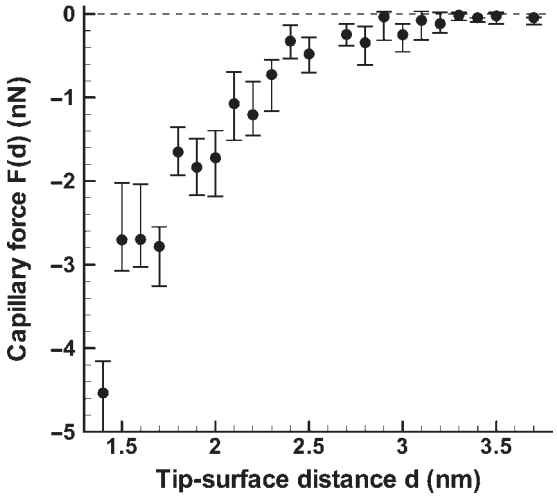

Figure 5. The capillary force $F(d)$ versus the tip–surface distance d. For each tip–surface distance, r_1 and r_2 are estimated from the density profile as in Figure 3, and then we use Equation (4) to calculate $F(d)$ (circles). Error bars represent the fluctuations in the force due to the fluctuation in r_2 of Figure 4. The tip and surface are both hydrophilic ($\varepsilon_{TO}/\varepsilon_{OO} = \varepsilon_{SO}/\varepsilon_{OO} = 3.6$).

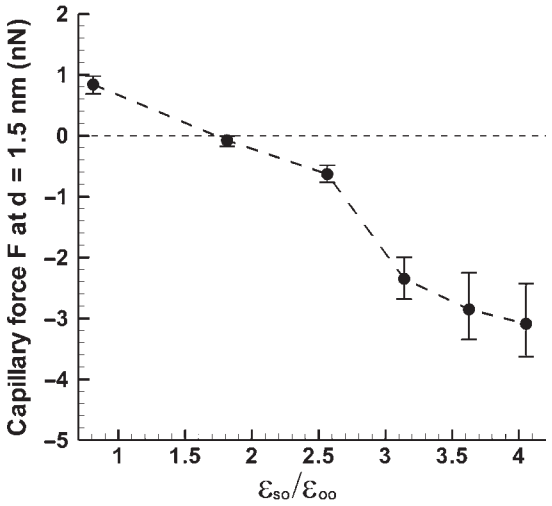

Figure 6. Capillary force F on a hydrophilic tip as a function of the surface hydrophilicity $\varepsilon_{SO}/\varepsilon_{OO}$. The fluctuation in the force due to the fluctuation in r_2 is drawn as error bars. The hydrophilic tip energy parameter is fixed as $\varepsilon_{TO}/\varepsilon_{OO} = 4$. The degree of surface hydrophilicity $\varepsilon_{SO}/\varepsilon_{OO}$ (hydrophilic if greater than 1) is varied. Negative (positive) values represent attractive (repulsive) forces. For each ε_{TO}–ε_{SO} combination, we calculated the capillary force (drawn as circles) at the tip–surface distance of 1.5 nm. Connecting lines between the data points and the horizontal line are drawn to guide eyes.

experiment. On the whole, the capillary force increases with raising the tip–surface distance. It is the most attractive at the shortest tip–surface distance, and disappears at the distance of 3.3 nm due to the breakage of the meniscus. The force sometimes decreases little bit (about 0.2 nN) locally as we increase the tip–surface distance. Considering the statistical uncertainty represented by error bars, however, we can say that the force is an increasing function of the tip–surface distance. In addition, regardless of d, the meniscus periphery is often far from a circle in shape (as we saw in Figure 2(b)). This circular approximation also might contribute to this erratic local behaviour of the force with respect to d.

Figure 6 illustrates the effects of the surface hydrophilicity on the capillary force. Here, the tip–surface distance is fixed to 1.5 nm and the tip is hydrophilic ($\varepsilon_{TO}/\varepsilon_{OO} = 4.1$). Then we have varied the relative strength of the molecule–surface interaction, $\varepsilon_{SO}/\varepsilon_{OO}$, as 0.8, 1.8, 2.6, 3.6 and 4.1. For the hydrophobic surface ($\varepsilon_{SO}/\varepsilon_{OO} = 0.8$), the capillary force is repulsive due to the convex ($r_1 > 0$) shape of the meniscus. As the surface becomes weakly hydrophilic ($\varepsilon_{SO}/\varepsilon_{OO} = 1.8$), the capillary force becomes slightly attractive. A further increase in ε_{SO} makes the capillary force more and more attractive. The molecular origin of this behaviour is as follows. For all the hydrophilic surfaces in Figure 6, the meniscus neck radius is nearly identical ($r_2 \sim 3$ nm). As the surface becomes more hydrophilic ($\varepsilon_{SO}/\varepsilon_{OO}$ varying from 1.8 to 4.1), the meniscus periphery becomes more curved (r_1 becomes smaller, changing from 3 to 0.56 nm) to give a more attractive capillary force. Our criterion for hydrophilicity has been based on the relative magnitude of the LJ energy parameters of molecule–surface and intermolecular interactions. A better criterion would be the microscopic contact angle of a water droplet on the surface [24]. Therefore, we have simulated a water droplet on the surface for various energetic parameters. By using the same number of water molecules as in the meniscus simulation, we obtained the density profile of droplet similar to Figure 3. Then we least-squares fit the 0.5 contour line of the density profile with a circle. Then the contact angle is defined as the angle between the tangential line at the crossing point of the circle and the flat surface. We found that the corresponding contact angles are 126°, 89°, 55°, 23° and 14°, $\varepsilon_{SO}/\varepsilon_{OO} = 0.8$, 1.8, 2.6, 3.1 and 3.6, respectively. Therefore, these contact angles are consistent with our classification of hydrophilicity using the ratio of LJ epsilon values.

One might argue that, due to the lattice-like initial configuration, our simulation should be regarded as the liquid (or evaporation) branch of the meniscus. If there is a hysteresis in the gas–liquid (or condensation–evaporation) transition, our meniscus could be different from the one from the gas branch. Our meniscus, however, is confined vertically (less than 4 nm) between the tip and the surface, and is finite in its lateral dimension (less than 8 nm) as well. It is well known that such a small pore does not show any hysteresis [25,26]. Moreover, our simulation has a typical length of MD trajectory for study

of adsorption in porous materials [27]. Therefore, our simulation should be able to reproduce the equilibrium structure of the nanometre meniscus.

We stress that the present work focuses on the structural properties of meniscus. In our NVT MD simulation, the relative humidity (vapour pressure) is not a fixed input but has to be calculated by running simulation. For simplicity, we used the Kelvin equation to get the vapour pressure and the capillary force. Such calculation gives relative humidity fluctuating around 70%. Although the use of the macroscopic Kelvin equation can be problematic, the meniscus structure should be a rigorous molecular simulation result.

Instead of the Kelvin equation, one might look for a molecular approach to calculate the capillary force. One convenient way is to check the total energy of our system as we vary the tip–surface distance. The derivative of energy with respect to distance will give capillary force to a first-order approximation (in general, there will be an entropic contribution too). We calculated such force by fitting the distance-dependent energy to an exponential function of distance. Then the capillary force was obtained by taking derivative of the fitting function. The resulting force shows a curve quite similar to Figure 5. The difference in the force is mostly 1 or 2 nN and it becomes smaller as the tip–surface distance increases.

Equation (4) expresses the capillary force due to the pressure difference between inside and outside of the water meniscus. There is additional contribution to the force arising from the surface tension of the meniscus given by $2\pi r_2 \gamma \sin(\theta_h)$, where θ_h is the angle between the meniscus and the horizontal line passing through the crossing point of the meniscus and the tip [28]. When we calculated the surface tension force, we found its magnitude to be about 1 nN at the most. If we plot the surface tension force as a function of the tip–surface distance, it becomes merely a small, near-constant background to the force in Figure 5. Therefore, we conclude that the surface tension force is negligible in our simulation.

4. Conclusions

We completed an all-atom MD simulation of the water meniscus formed between an AFM tip and a surface. Such a nanoscale meniscus is ubiquitous in AFM experiment and direct-write nanolithography, but we poorly understand its molecular property. We examined how the meniscus structure varies as the distance between the tip and the surface changes. Overall, the meniscus shrinks in its width as the tip retracts from the surface, eventually snapping off as the tip–surface distance further increases. We obtained the density profile of water for various tip–surface distances. The meniscus periphery obtained from the molecular density profile is not infinitely sharp but rather fuzzy with a thickness ranging from 0.4 to 0.9 nm. The density profile also provides the structural parameters of the meniscus, i.e. its neck radius r_2 and the radius of curvature of its periphery r_1. The meniscus periphery sometimes could not be approximated as a circle, especially for narrow (less than 0.5 nm in neck radius) menisci. For our nanoscale menisci, r_2 and r_1 were comparable in size. This is in contrast to the case of a macroscopic tip (with a large radius), where r_2 is much greater than r_1. With the structural parameters, we can calculate the capillary force by using the Laplace–Kelvin equation. Such a hybrid approach gives the capillary force versus the tip–surface distance in qualitative agreement with typical AFM experiment. The capillary force becomes more attractive as we increase the surface hydrophilicity. This is due to the fact that the radius of curvature of the meniscus periphery decreases as the surface becomes more hydrophilic.

Our tip and surface atoms have the size of a carbon atom. Their energetic parameters have been arbitrarily set and varied to see the effects of tip and surface hydrophilicity. For this rather artificial system, a quantitative comparison with experiment seems difficult. In addition, the exact tip and surface geometries required for a simulation of a specific experiment are not known. We here content ourselves with the fact that our capillary force reproduces the typical magnitude of pull-off force measurement (several nN) [8].

Hopefully, the current work serves as a starting point for further investigation of the nanoscale meniscus and the capillary force at the molecular level. In the future, we would like to use a fully molecular theory for the capillary force, obviating the use of the macroscopic Laplace–Kelvin equation and the circular approximation for the meniscus periphery. For example, combining the current MD with the venerable density functional theory [29] would be a viable option to calculate the capillary force. Such an effort will foster fundamental understanding of the humidity induced adhesion in AFM and of the optimal control of direct-writing nanolithography.

Acknowledgements

This work was supported by the Korea Research Foundation Grant funded by the Korean Government (MOEHRD, Basic Research Promotion Fund; KRF-2008-521-C00123)

References

[1] B.L. Weeks, M.W. Vaughn, and J.J. DeYoreo, *Direct imaging of meniscus formation in atomic force microscopy using environmental scanning electron microscopy*, Langmuir 21 (2005), pp. 8096–8098.

[2] K.B. Jinesh and J.W.M. Frenken, *Capillary condensation in atomic scale friction: how water acts like a glue*, Phys. Rev. Lett. 96 (2006), 166103.

[3] S.H. Yang, M. Nosonovsky, H. Zhang, and K.-H. Chung, *Nanoscale water capillary bridges under deeply negative pressure*, Chem. Phys. Lett. 451 (2008), pp. 88–92.

[4] J.N. Israelachvili, *Intermolecular and Surface Forces*, 2nd ed., Academic Press, London, 1991.
[5] L.D. Gelb, K.E. Gubbins, R. Radhakrishnan, and M. Sliwinska-Bartkwiak, *Phase seperation in confined systems*, Rep. Prog. Phys. 62 (1999), pp. 1573–1659.
[6] D.-I. Kim, J. Grobelny, N. Pradeep, and R.F. Cook, *Origin of adhesion in humid air*, Langmuir 24 (2008), pp. 1873–1877.
[7] R. Jones, H.M. Pollock, J.A.S. Cleaver, and C.S. Hodges, *Adhesion forces between glass and silicon surfaces in air studied by AFM: effects of relative humidity, particle size, roughness, and surface treatment*, Langmuir 18 (2002), pp. 8045–8055.
[8] D.L. Sedin and K.L. Rowlen, *Adhesion forces measured by atomic force microscopy in humid air*, Anal. Chem. 72 (2000), pp. 2183–2189.
[9] X. Xiao and L. Qian, *Investigation of humidity-dependent capillary force*, Langmuir 16 (2000), pp. 8153–8158.
[10] C.A. Mirkin, *The power of the pen: development of massively parallel dip-pen nanolithography*, ACS Nano 1 (2007), pp. 79–83.
[11] T. Stifter, O. Marti, and B. Bhushan, *Theoretical investigation of the distance dependence of capillary and van der Waals forces in scanning force microscopy*, Phys. Rev. B 62 (2000), pp. 13667–13673.
[12] J. Jang, G.C. Schatz, and M.A. Ratner, *How narrow can a meniscus be?*, Phys. Rev. Lett. 92 (2004), 085504.
[13] J. Jang, J. Sung, and G.C. Schatz, *Influence of surface roughness on the pull-off force in atomic force microscopy*, J. Phys. Chem. C 111 (2007), pp. 4648–4654.
[14] J. Jang, M. Yang, and G.C. Schatz, *Microscopic origin of the humidity dependence of the adhesion force in atomic force microscopic*, J. Chem. Phys. 126 (2007), 174705.
[15] L. Maibaum and D. Chandler, *A coarse-grained model of water confined in a hydrophobic tube*, J. Phys. Chem. B 107 (2003), pp. 1189–1193.
[16] T. Cramer, F. Zerbetto, and R. Garcia, *Molecular mechanism of water bridge buildup: field-induced formation of nanoscale menisci*, Langmuir 24 (2008), pp. 6116–6120.
[17] M.P. Allen and D.J. Tildesley, *Computer Simulation of Liquids*, Clarendon Press, Oxford, 1987.
[18] W.L. Jorgensen, J. Chandrasekhar, J.D. Madura, R.W. Impey, and M.L. Klein, *Comparison of simple potential functions for simulating liquid water*, J. Chem. Phys. 79 (1983), pp. 926–935.
[19] T. Darden, D. York, and L. Pederson, *Particle mesh Ewald: an N-log(N) method for Ewald sums in large systems*, J. Chem. Phys. 98 (1993), pp. 10089–10092.
[20] R. Kubo, M. Toda, and N. Hashitsume, *Statistical Physics II: Nonequilibrium Statistical Mechanic*, 2nd ed., Springer, Berlin, 1985.
[21] C. Phillips, R. Braun, W. Wang, J. Gumbart, E. Tajkhorshid, E. Villa, C. Chipot, R.D. Skeel, L. Kale, and K. Schulten, *Scalable molecular dynamics with NAMD*, J. Comp. Chem. 26 (2005), pp. 1781–1802.
[22] J. Jang, G.C. Schatz, and M.A. Ratner, *Capillary force in atomic force microscopy*, J. Chem. Phys. 120 (2004), pp. 1157–1160.
[23] L. Sirghi, N. Nakagiri, K. Sugisaki, H. Sugimura, and O. Takai, *Effect of sample topography on adhesive force in atomic force spectroscopy measurements in air*, Langmuir 16 (2000), pp. 7796–7800.
[24] E.R. Cruz-Chu, A. Aksimentiev, and K. Schulten, *Water-silica force field for simulating nanodevices*, J. Phys. Chem. B 110 (2006), pp. 21497–21508.
[25] Y.K. Tovbin, D.V. Yeremich, and L.K. Zhidkova, *Vapour-liquid coexisting curves and hysteresis of simple adsorbate in complex porous systems*, Appl. Surf. Sci. 252 (2005), pp. 591–601.
[26] A.V. Neimark, P.I. Ravikovitch, and A. Vishnyakov, *Adsorption hysteresis in nanopores*, Phys. Rev. E 62 (2000), pp. R1493–R1496.
[27] L. Sarkisov and P.A. Monson, *Hysteresis in Monte Carlo and molecular dynamics simulations of adsorption in porous materials*, Langmuir 16 (2000), pp. 9857–9860.
[28] A. de Lazzer, M. Dreyer, and H.J. Rath, *Particle-surface capillary force*, Langmuir 15 (1999), pp. 4551–4559.
[29] P.B. Paramonov and S.F. Lyuksyutov, *Density-functional description of water condensation in proximity of nanoscale asperity*, J. Chem. Phys. 123 (2005), 084705.